applied sciences

MDPI

Article

Estimation of the Wind Load Required to Cause the Overturning of a Gantry Crane, Comparing Different Structures of the Main Horizontal Girder

Marcin Augustyn * and **Marek Barski**

Department of Machine Design and Composite Structure, Faculty of Mechanical Engineering, Cracow University of Technology, Al. Jana Pawła II 37, 31-864 Kraków, Poland; marek.barski@pk.edu.pl

* Correspondence: marcin.augustyn@pk.edu.pl

Abstract: The present paper concerns the problem of estimating the loading induced by the wind on a gantry crane standing in the open air. Sufficiently strong wind may cause the device to move or even tip over. Two different structures were studied, namely the box girder and truss girder. At the very beginning, the two sectional scaled parts of the main horizontal beam (box and truss girder) of the gantry were prepared. Next, experimental analysis using these models was carried out in an aerodynamic tunnel to estimate the horizontal forces induced by the airflow acting on them. The experimental values of the aerodynamic forces were exploited to verify the 3D computational model of the studied structure. Numerical computations were carried out using the ANSYS Fluent 2022R2 system for both sectional models of the gantry crane mentioned above. The standard k-epsilon model of the turbulent flow of the air is employed. Satisfactory agreement of the values between the experimental and numerical results was achieved. As a result of the performed computations, the magnitude of the critical wind velocity that can be dangerous for the studied gantry cranes was estimated. Finally, a model of the gantry crane with box girder at full scale was analyzed using CFD simulations for different Davenport wind profiles. The results obtained from the experimental and numerical analysis of the sectional models were compared with the appropriate standards. In the current work, attention is drawn to the importance of changing wind direction in the vertical plane since, as shown in the results of this work, even a small change in vertical angle, up to 6°, causes significant changes in the value of the force required to overturn the gantry crane.

Keywords: wind loading; gantry crane; box girder; truss girder; CFD; aerodynamic tunnel; tip-over

Citation: Augustyn, M.; Barski, M. Estimation of the Wind Load Required to Cause the Overturning of a Gantry Crane, Comparing Different Structures of the Main Horizontal Girder. *Appl. Sci.* **2024**, *14*, 1092. https://doi.org/10.3390/app14031092

Academic Editor: Igal M. Shohet

Received: 28 December 2023
Revised: 18 January 2024
Accepted: 18 January 2024
Published: 27 January 2024

1. Introduction

With the rapid change in climate conditions, the phenomena associated with strong winds are becoming more dangerous. Moreover, early wind prediction is also becoming more difficult. An example is the category 5 Hurricane Otis [1], which devastated Acapulco city in Mexico on 25 October 2023. At the very beginning, this hurricane was estimated as only a tropical storm, but unexpectedly, it became an unusually strong hurricane. The wind blew at 265 km/h. Sudden gusts of wind were even stronger. The observed wind gust speed was equal to 330 km/h. Equally dangerous weather phenomena also occur in previously moderate climate zones. At the beginning of November 2023, Europe was hit by Hurricane Ciaran [2]. The wind gust speed exceeded 200 km/h. In such conditions, all types of lifting equipment, such as scissor lifts, elevating work platforms of different kinds, and cranes, including tower cranes, are particularly vulnerable to destruction [3–11]. This paper examines the problem of the wind load acting on the gantry crane, particularly how strong the wind must be to cause the whole structure to tip over. Gantry cranes seem very stable and resistant to strong gusts of wind. However, cases of this type of structure overturning due to strong winds have been known to occur [12,13].

The wind load is considered one of the most important loads in the design process. It is found in many codes, such as [14–19]. The European Standard ISO-4302 [14] (like the other cited standards) concerns wind loading in cranes. According to the standard, if the wind blows at a constant speed from any horizontal direction, it will cause a quasi-static uniform load (pressure) on the investigated structure. This approach should be treated as a relatively simple method. The calculation method also considers redundancy qualities, considering the effects of gusts (rapid changes in wind speed) and the dynamic response of the crane structure. When calculating wind for cranes, two load states are considered.

The first is the wind load for cranes in the working state. This is the highest wind load that acts on the crane during its operation and for which it was designed. The wind load is assumed to act from the least favorable direction in combination with other operating loads. According to the code [14], the operating state wind speeds and corresponding pressures are as follows: if the crane manufacturer has not adopted and specified other values in the crane's operating instructions, then, in the case of normal cranes working in open space, the design wind speed is equal to V = 20 m/s, and the corresponding wind design wind pressure is p = 250 N/m^2, whereas in the case of cranes that must work in high winds, the design wind speed and design wind pressure are equal to V = 28.5 m/s and p = 500 N/m^2, respectively.

The second crane load condition, according to [14], is the wind load on cranes in the non-working state. This is the strongest (storm) wind gust load from the least favorable direction that acts on the crane in the non-working state and for which the crane was designed. The wind speed is variable and depends on the geographic location and the degree of exposure of the crane to the wind.

Regardless of the code, however, the following equation is used to calculate wind load F of the entire crane, its parts, and individual structural elements [14]:

$$F = A \cdot p \cdot C_f, \tag{1}$$

where A is the effective frontal area of the part under consideration in m^2, i.e., the area of the projection of all elements on a plane, which is perpendicular to the wind direction; p denotes the wind pressure; and C_f is the streamlining coefficient of the part under consideration in the direction of the wind action.

When calculating the wind load of a crane in a non-swinging state, the wind pressure is assumed to have a constant value in each 10 m vertical height interval of the crane. Alternatively, wind pressure can be calculated at locations at any height, or a constant value of wind pressure calculated for the highest point on the structure can be assumed.

The resultant wind load acting on a structure is the sum of the loads on the individual components. In the case when the direction of the wind is not parallel to the longitudinal axis of the component or frame surface, the magnitude of the aerodynamic force is estimated with the use of the following expression:

$$F = A \cdot p \cdot C_f \cdot sin^2\theta, \tag{2}$$

in which θ is the angle between the wind direction and the longitudinal axis or surface (θ < 90°). However, it should be stressed that the approach presented in the mentioned standards could be inadequate compared to real-life conditions. This is mainly due to different additional phenomena like vibrations, interference with the neighboring buildings and structures, etc. Therefore, works that report the results of the measured wind conditions performed on real-scale structures are very important [20–22]. Next, these results are the basis for creating appropriate conditions in the aerodynamic tunnels, where the scaled models or parts of real-scale structures are investigated [23–26].

The rapid evolution of finite element software enables performing numerical analyses of more and more complicated problems which concern the phenomena of the airflow around and through crane-like engineering structures for different wind profiles [27–29]. Further mechanical analysis is possible when the distribution of the wind-induced load on the analyzed structure is available. Finally, the displacement or stress distribution in the most important nodes of the structure can be estimated [30]. However, other approaches in computer science are also developed to determine the stability margin during lift operations, for example, Romanello [31]. El Ouni et al. [32] proposed and designed an active system of actuators and sensors for the mitigation of the dangerous effects of wind on the crane. Chen et al. [33] prepared a mathematical model for the evaluation of the wind coefficients for the tower crane.

As mentioned above, a particularly dangerous situation is when a sudden gust of wind acts on the crane structure with a payload during the operation service, for example, as demonstrated by Skelton et al. [34] and Cekus et al. [35,36].

The direct motivation for this work is the below-described accidents. It is worth noting that the wind damage, primarily involving cranes being blown along rails, is the highest damage cost. For example, in the accident at the LNG gas terminal in Świnoujście (Poland) in 2017 [37], not only the crane was damaged but also the critical infrastructure in the immediate vicinity. The dome of the eastern gas tank and a section of the pipeline were damaged. An example of a gantry crane accident with a box girder, which was destroyed due to exceptionally high wind, is a large gantry crane at the Damen ship repair yard in Schiedam, near Rotterdam, The Netherlands, in 2018 [38]. According to media information, the crane was properly secured, but one side of the crane began moving, causing a twist that broke the girder away from its supports. Witnesses to this event claim that the high winds may have created a localized tornado effect. Another accident involves the case of the gantry crane with a truss girder described in the work of Frendo [13].

In the present work, two kinds of gantry cranes are studied: a gantry with a box girder and a gantry with a truss girder. For both structures, we prepared the scaled sectional models of the main horizontal girders (box girder and truss girder). Next, we performed experimental tests in the aerodynamic tunnel to estimate the horizontal and vertical aerodynamic coefficients of these models. The results of these tests were exploited to verify these results, which were obtained from CFD simulations. After, computations were performed for the real structure, namely a gantry crane with a box girder, when the numerical model was verified. These calculations aim to evaluate the magnitude of the wind speed, which causes the whole structure to tip over. An appropriate research framework diagram is depicted in Figure 1.

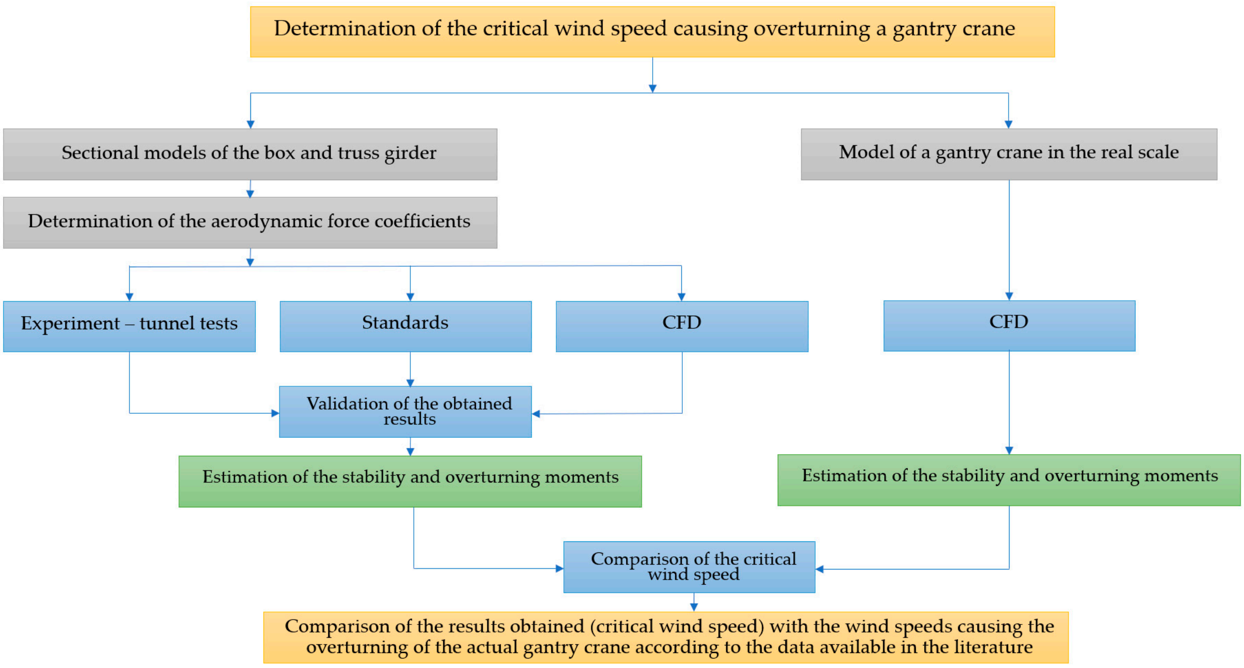

Figure 1. The research framework diagram.

It should be stressed that performing the CFD simulation is very difficult for gantry cranes with the horizontal truss girder. It is mainly caused by the fact that the appropriate mesh must consist of a significantly large number of elements with proper geometry. Often, it is very difficult; therefore, the aerodynamic forces and wind speed causing overturning for this kind of structure are estimated based on the sectional model. The obtained results are confronted with appropriate standards. It should be noted that this work is a continuation of the problems presented in the previous papers [38,39].

2. Materials and Methods

2.1. Analysis Object

The currently presented work concerns the investigations of two gantry cranes, namely a gantry with a horizontal box girder, SBS-8, and a gantry with a horizontal truss girder, SBS-4.5, designed and produced by the Polish factory ZREMB. Both structures are shown in Figure 2a,b.

(**a**) (**b**)

Figure 2. The real research objects: (**a**) the gantry crane SB-8 with box girder; (**b**) the gantry crane SBS-4.5 with truss girder.

The gantry cranes, which are the subject of investigation, consist of one girder suspended on two supports equipped with a rail-type chassis. The structure does not need to be constructed in a manufacturing place but can work indoors and outdoors due to mobile support. The basic element of the gantry crane's supporting structure is the girder, which is made of welded sheet metal or a truss (Figure 2a,b). The girder carries the loads that arise during the operation of the gantry crane and is also exposed to strong gusts of wind.

The box girder of the SB-8 gantry crane and the truss girder of the SBS-4.5 gantry crane were selected for experimental wind impact studies in the wind tunnel. The overall dimensions of both gantry cranes are presented in Figure 3a,b. The basic technical parameters of the above-mentioned gantry cranes are listed in Table 1.

Table 1. Basic technical parameters of studied gantry crane.

	SB-8	**SBS-4**	
Capacity	8	4.5	(tons)
Span	5.75 + 16 + 5.75	3.825 + 10 + 3.825	(m)
Lift height	8.0	6.0	(m)

2.2. Sectional Models of the Girder

In the first steps of the numerical and experimental investigations, the scaled sectional models of the box girder "B" and truss girder "T" are involved. Sectional models represent the part of the horizontal girder of a gantry crane and are based on the dimensions of real objects. Because of the dimensions of the wind tunnel measurement space, the geometric scale of the models was adopted as 1:8.5. The models' basic dimensions are shown in Figure 4a,b.

According to the dimensions of the scaled models, shown in Figure 4a,b, the corresponding physical models used in the experimental and numerical models for CFD simulation were prepared. The finished models are shown in Figures 5 and 6.

Structural steel was used to make the models, and the structural elements of the box girder and the lattice girder section were connected by welding. The two models for experimental testing were closed on both sides, with an aluminum disc of diameter D = 400 mm and thickness t = 4 mm. The round plates dissipate air turbulence at the ends of the cross-sectional models. The holders allow the models to connect to the measuring device (three-component aerodynamic balance). For numerical models, the corresponding holders are not necessary.

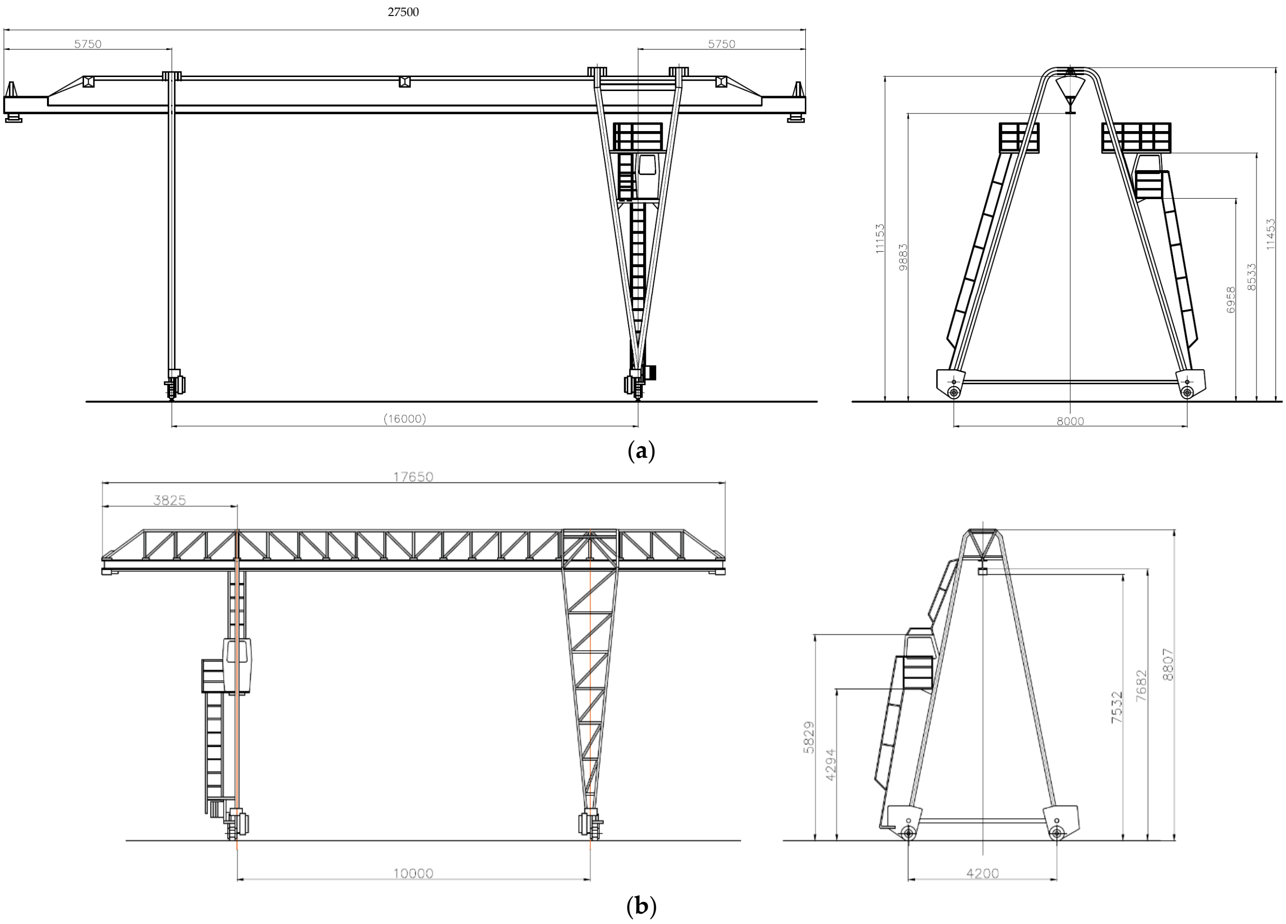

Figure 3. The geometrical dimensions of (**a**) the gantry crane SB-8 and (**b**) the gantry crane SBS-4.5.

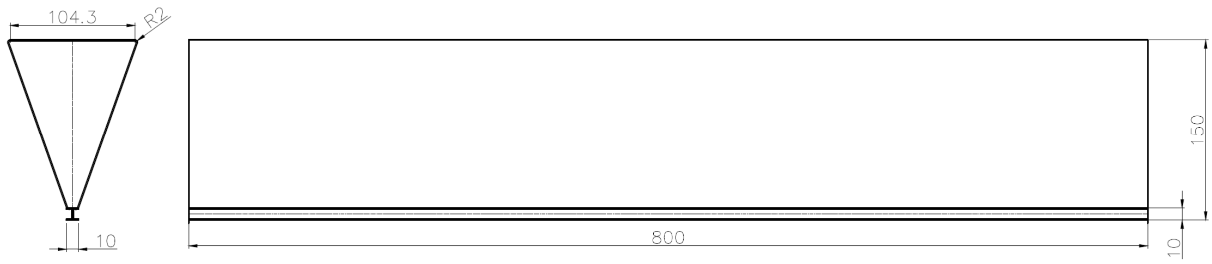

(**a**)

Figure 4. *Cont.*

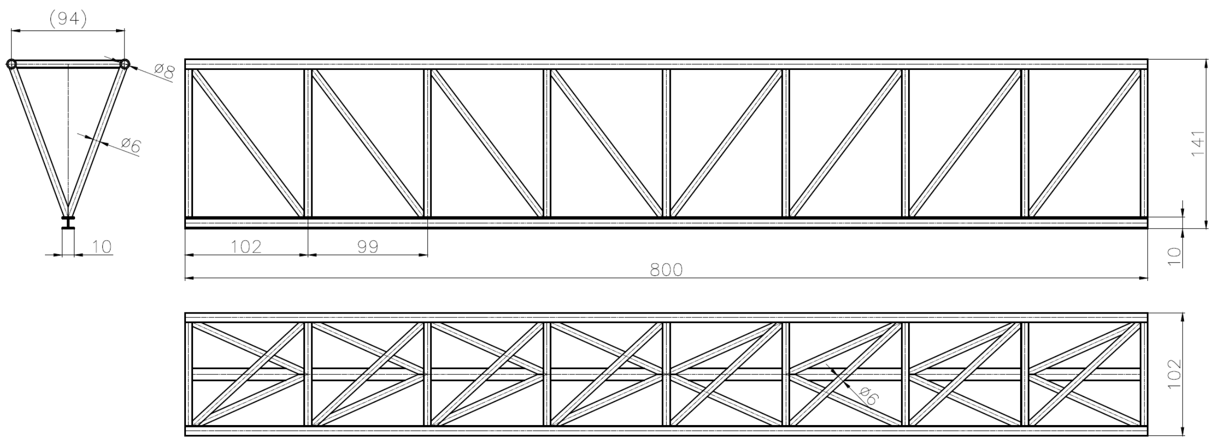

(**b**)

Figure 4. The overall dimension of the scaled section model: (**a**) model of box girder SB-8; (**b**) model of truss girder SB-4.5.

(**a**)

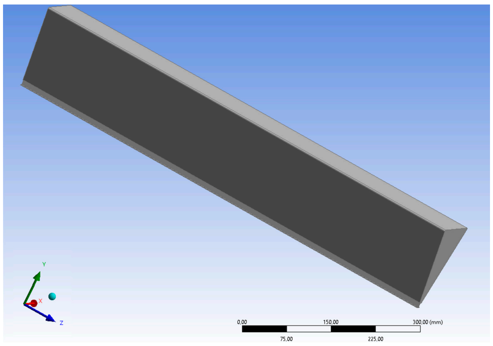

(**b**)

Figure 5. The model of the box girder of the SB-8: (**a**) for experimental tests; (**b**) for CFD simulation.

(**a**)

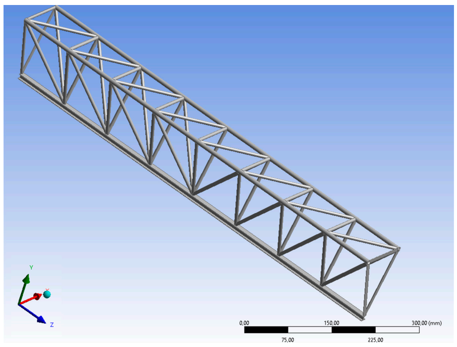

(**b**)

Figure 6. The model of the truss girder of the SB-4.5: (**a**) for experimental tests; (**b**) for CFD simulation.

2.3. Experimental Setup

Experimental studies were carried out at the Wind Engineering Laboratory of the Cracow University of Technology [40]. The aerodynamic tunnel allows for a maximum wind speed of about 40 m/s in a measuring area of 10 m in length. The flow can take place in both closed and open circuits. The shape of the measurement space is rectangular and is 2.2 m wide and 1.4 m high.

A closed-circuit tunnel was used during the test. The first 6 m of the measurement space is intended to create a profile of wind speed and induce turbulent flow. For this purpose, a barrier, and spires of appropriate geometry and spacing were used. The barrier is 200 mm high, and its top edge is irregular and zigzag. The spires are pyramid-shaped.

The width at the base is 300 mm, and the height is 1000 mm. Both elements are located at the tunnel close to the inlet, as shown in Figure 7a. The flat urban terrain and turbulent flow are assumed.

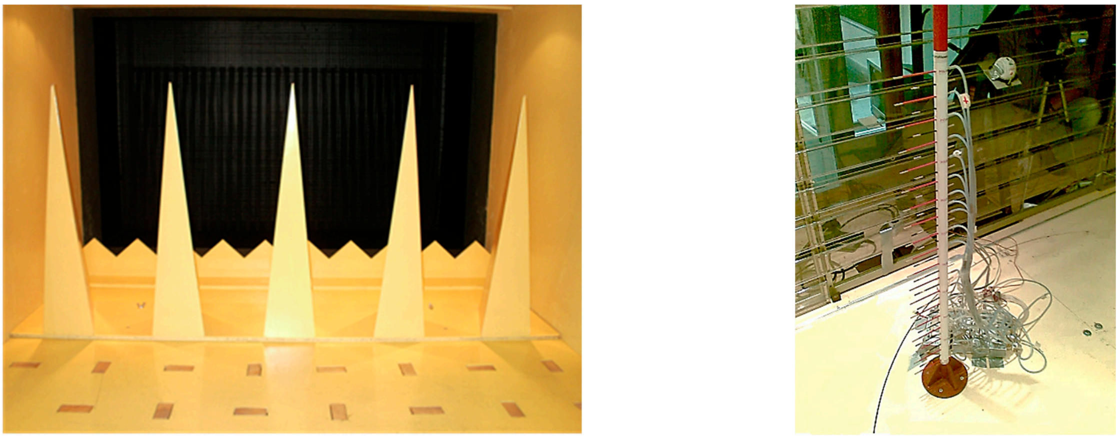

(**a**) (**b**)

Figure 7. Elements of tunnel equipment: (**a**) spires and a barrier for generating turbulent flow; (**b**) vertical rod with pressure sensors for determining the wind profile.

The wind speed measurement was carried out using a set of pressure sensors, as shown in Figure 7b. The wind profile was determined independently in the tunnel without the investigated sectional models. Next, the appropriate model was installed inside the tunnel, and the measurements were performed. For these settings, the wind profile was determined at heights between 200 and 700 mm above the floor of the tunnel using six anemometers placed vertically at 100 mm. The height range was determined by the location of the model in the measurement space. The sectional models were placed 350 mm above the tunnel floor. Therefore, the mean value of wind speed V_{ref} = 17.01 m/s was assumed at a 400 mm height (mean value of dynamic pressure p_{ref} = 181.59 N/m^2). Turbulence intensity I_V = 12.7% and is the quotient of the standard deviation of the measured wind speed σ_v and the mean value of wind speed V_{ref}. The resulting wind profile and turbulence intensity are shown in Figure 8a,b.

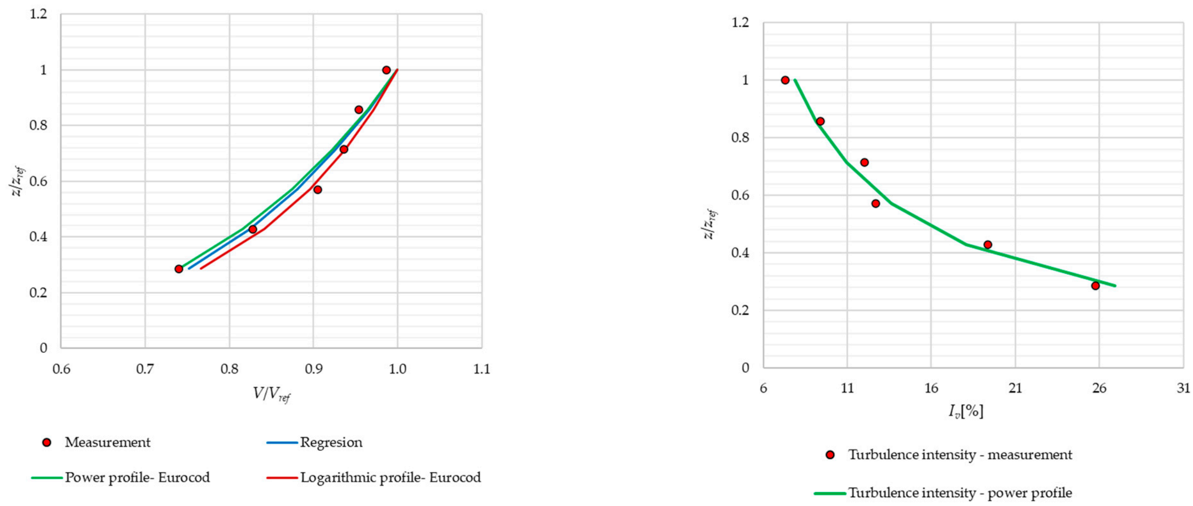

(**a**) (**b**)

Figure 8. Characteristics of (**a**) the wind speed profile for urban terrain and (**b**) the turbulent intensity profile for urban terrain [41].

The coordinate system and the method for defining the wind direction angle θ are shown in Figure 9. For the models tested in the tunnel, the aerodynamic forces F_x and F_y and the aerodynamic moment M_{xy} are measured using a three-component balance based on the electrical resistance of the strain gauges. The fixed x, y, and z coordinate system is as follows: x—along the wind direction, y—across the wind direction, and z—in the vertical direction; W—wind direction, with changes from $-6°$–$6°$ in $1°$ increments.

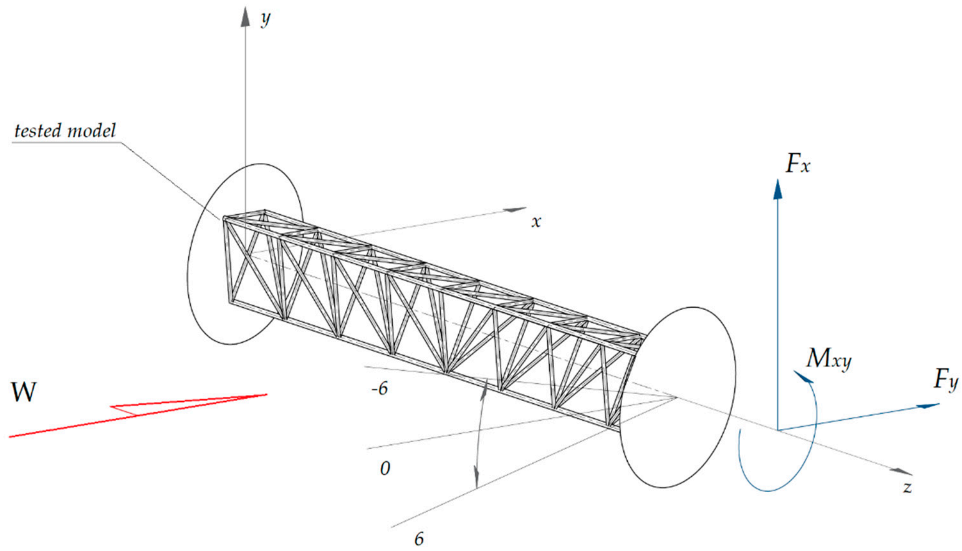

Figure 9. The wind direction and assumed Cartesian coordinate system used in the experiment.

The model of the studied girder of the gantry crane was installed horizontally onto the aerodynamic balance. The angle of the wind direction θ was changed by rotating the model in the xy plane. A diagram of the measuring system is depicted in Figure 10.

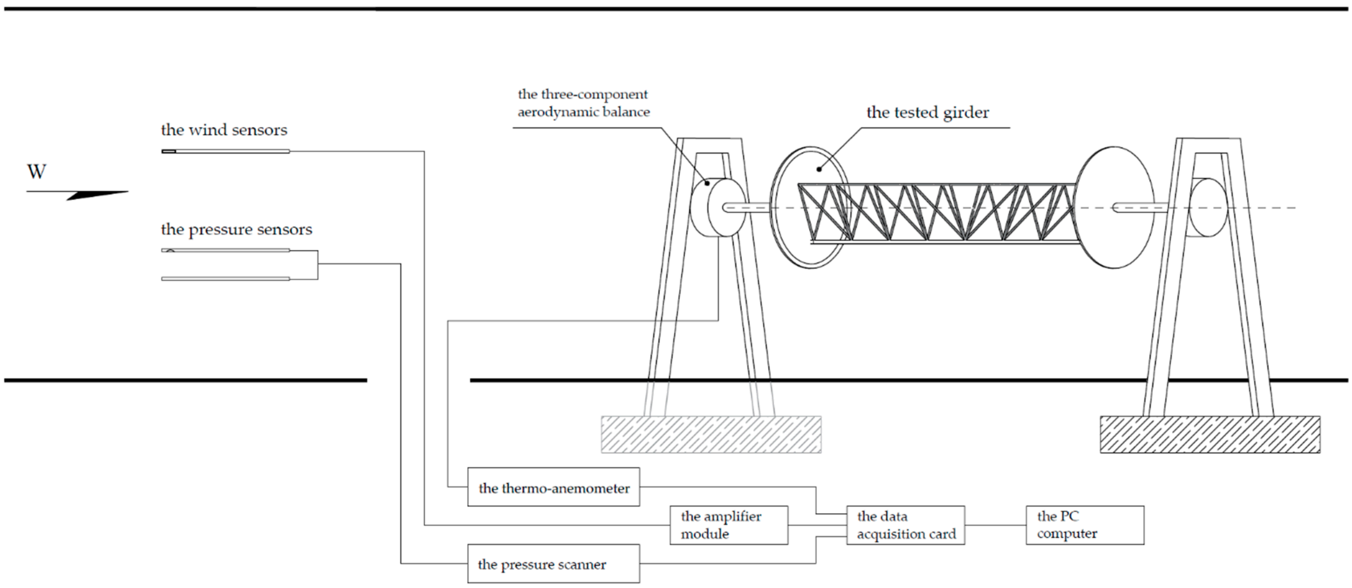

Figure 10. Diagram of the measuring system.

To preview the wind speed value in real time, a wind speed sensor with a thermoanemometer was also used to measure the wind speed. The sampling time of the experimental data was equal to 5000 ms.

2.4. CFD Simulation

Scaled Sectional Models

The CFD analysis was performed to estimate the magnitude of the aerodynamic forces acting on the studied sectional models of the gantry crane and the whole gantry (in the real scale) crane. The numerical simulations were carried out with the commercially available software ANSYS FLUENT 2022R2. All performed simulations were performed under the assumption of the steady state of the airflow. Moreover, the standard air properties (density, temperature, ambient pressure, and viscosity) were also assumed, namely ρ = 1.225 kg/m^3, p_0 = 101,325.25 Pa, and $\mu = 1.7894 \times 10^{-5}$ Pa s, and T = 15 °C.

The CFD computations in the case of the scaled sectional models were performed under the assumption that the simulations recreate the conditions in the aerodynamic tunnel. The transversal dimensions of the measurement are 2200 × 1400 mm. The length of the considered part of the aerodynamic tunnel is equal to L_t= 2500 mm. The sectional models were placed at a distance L_1 = 1000 m from the inlet (Figure 11a,b, where the inlet is shown as a blue wall).

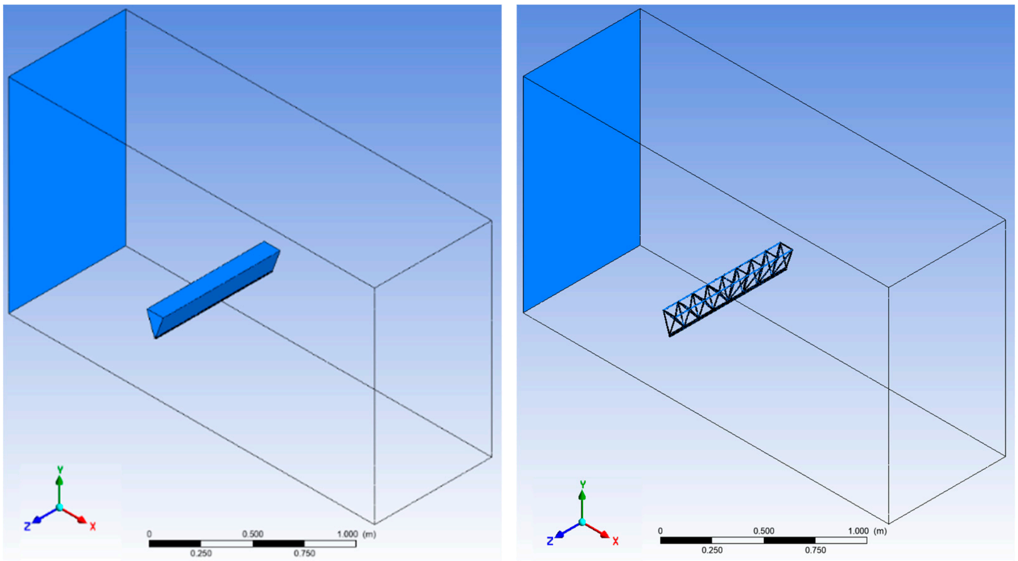

(**a**) (**b**)

Figure 11. Studied sectional models immersed in the volume filled with the air: (**a**) box girder; (**b**) truss girder.

We decided to use the standard k-ε model because the dominant effect is the aerodynamic drag in the current work. This model of turbulent flow ensures relatively accurate precision when predicting aerodynamic forces under the assumption of ideal rigidity of the investigated models of structures. Moreover, this model has been successfully used in different works [29,38,39,42,43].

However, it is worth noting that besides the k- ε model, the following models are exploited, namely the Reynolds stress model and k-omega model. The Reynolds model [44] can cause significant problems with computation convergence, and the computation process is prolonged. On the other hand, the k-ω model [45–47] demands creating a special mesh of finite cells at the stationary boundaries, which consists of very small elements. Consequently, it causes the number of cells, nodes, and degrees of freedom to be significantly large. Moreover, this model has several variants that can, unfortunately, generate completely different results depending on the problem.

Figure 12a,b shows the meshes generated for the box and truss girders, respectively. For the box girder model, the approximate size of the tetrahedral elements varies from l_c = 2.5 mm to l_c = 60 mm. The total number of cells is equal to 2,763,302, and the total number of nodes is 689,675. For the model of the truss girder, the size of tetrahedral elements varies from l_c = 2 mm to l_c = 60 mm (3,646,476 cells and 889,314 nodes).

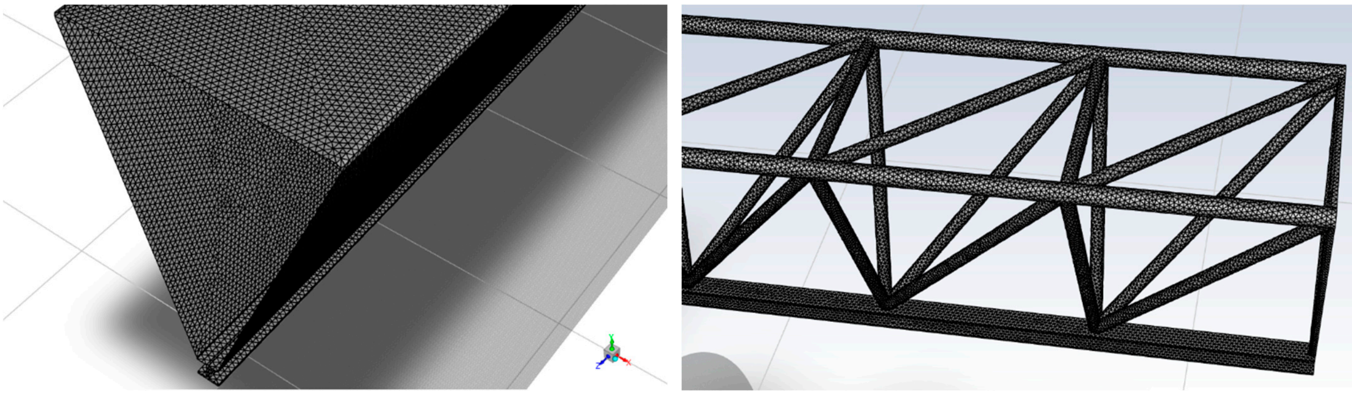

(**a**) (**b**)

Figure 12. The mesh created for (**a**) a sectional model of the box girder (length of the element edge l_c = 2.5 mm) and (**b**) a sectional model of the truss girder (length of the element edge l_c = 2 mm).

Several CFD simulations were performed with different sizes of the elements to estimate the impact of the element size on the aerodynamic forces. The convergent test was made for the sectional model of the box girder mainly due to the possibility of the change of size of the elements being strongly limited in the case of truss structures. The computations were performed for wind speed V = 17.1 m/s and a turbulence intensity of 12%. The hydraulic diameter is equal to D_H = 1.712 m. The wind direction (Figure 9) is assumed to be equal to θ = 0°. The results are reported in Table 2.

Table 2. Aerodynamic forces for different mesh.

Cell Size (mm)	Faces (Box Girder)	Nodes	Cells	F_x (N)	F_y (N)
1.5	14,251,914 (186,649)	1,698,020	6,655,980	38.605	20.094
2.5	5,857,993 (71,680)	689,675	2,743,302	38.491	20.035
3.5	4,923,579 (35,813)	571,922	2,312,836	37.077	18.521

As observed, the finite cell size equal to l_c = 2.5 mm seems to be optimal concerning the time of calculation and the obtained precision. To obtain a convergent solution, 111 iterations are required. However, the solution could not be converged concerning the assumed default criteria for larger elements. The problem is mainly caused by the continuity criterion. For the smaller elements, the obtained results differ not significantly, but the time of calculation (154 iterations) is radically and unacceptably longer.

3. Results

Aerodynamic forces obtained from experimental and numerical studies were used to determine the aerodynamic coefficients for the two girder models. The formulas for determining the drag coefficient C_x and the lateral force coefficient C_y are as follows:

$$C_x = \frac{2F_x}{\rho {V_{ref}}^2 \cdot A_{ref}},\ C_y = \frac{2F_y}{\rho {V_{ref}}^2 \cdot A_{ref}} \tag{3}$$

where A_{ref} is the effective area, which is A_{refB} = 0.112 m^2 for box girder model and A_{refT} = 0.028 m^2 for truss girder model.

3.1. Experimental and Numerical Results Obtained from CFD Simulation

Tables 3 and 4 summarize the values of the aerodynamic forces and coefficients obtained from the tunnel tests and CFD simulations for various angle θ (Figure 9) for gantry cranes with horizontal box and truss girders, respectively.

Table 3. Aerodynamic forces and coefficients of the box girder section model.

	Experiment				CFD			
θ (°)	**F_x (N)**	**F_y (N)**	**C_x**	**C_y**	**F_x (N)**	**F_y (N)**	**C_x**	**C_y**
−6	36.698	15.918	1.76	0.76	40.869	14.573	1.96	0.70
−4	37.621	13.905	1.80	0.67	40.157	16.494	1.92	0.79
−2	38.421	15.572	1.84	0.75	39.358	18.345	1.88	0.88
0	36.087	20.032	1.73	0.96	38.491	20.035	1.84	0.96
2	36.108	23.338	1.73	1.12	37.562	21.501	1.80	1.03
4	36.870	23.505	1.77	1.13	36.638	22.642	1.75	1.08
6	34.171	25.197	1.64	1.21	35.733	23.401	1.71	1.12

Table 4. Aerodynamic forces and coefficients of the truss girder section model.

	Experiment				CFD			
θ (°)	**F_x (N)**	**F_y (N)**	**C_x**	**C_y**	**F_x (N)**	**F_y (N)**	**C_x**	**C_y**
−6	12.050	0.082	2.54	0.02	10.487	0.310	2.21	0.07
−4	11.269	0.137	2.37	0.03	10.372	0.320	2.18	0.07
−2	11.110	0.037	2.34	0.01	10.303	0.343	2.17	0.07
0	10.351	0.740	2.18	0.16	10.256	0.430	2.16	0.09
2	10.606	1.007	2.23	0.21	10.248	0.561	2.16	0.12
4	10.991	1.628	2.31	0.34	10.267	0.713	2.16	0.15
6	12.176	1.564	2.56	0.33	10.335	0.846	2.17	0.18

In the case of the box girder, the aerodynamic drag force F_x slightly increases with increasing the angle theta. Contrary to drag force F_x, the aerodynamic lift force F_y decreases. However, the variations in the lift force F_y are much more significant. In Figure 13a,b, the selected results of CFD analysis for θ = 0° are shown.

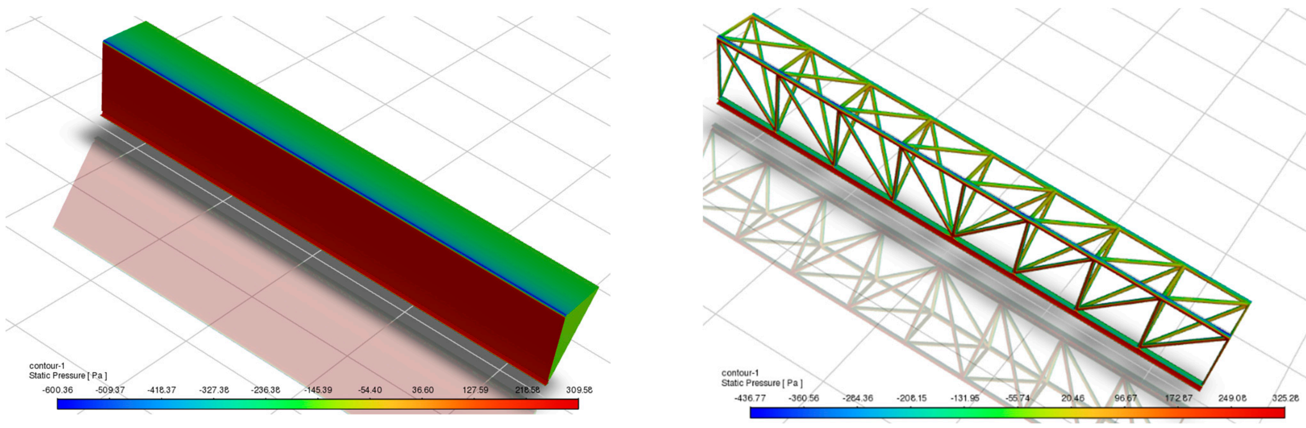

(**a**) (**b**)

Figure 13. Results of CFD analysis (θ = 0°): (**a**) distribution of the pressure for the box girder; (**b**) distribution of the pressure for the truss girder.

On the other hand, the wind direction impact in the studied angle range is negligible for the truss girder. The drag force F_x values are almost four times less than the box girder. The lift force F_y values are comparable with zero.

3.2. Experimental Verification of the CFD Results

To evaluate the agreement of the values of the resulting aerodynamic coefficients, the relative error is calculated using the following formula:

$$\varepsilon_{AVG} = \left| \frac{C_X^{exp} - C_X^{num}}{C_X^{num}} \right|, \tag{4}$$

where $C_x{}^{exp}$ is the aerodynamic force coefficient from the experiment, and $C_x{}^{num}$ is from the CFD, computed for the F_x component (Tables 3 and 4). In the case of the box girder, the average error does not exceed 5%, and the maximal value of the relative error, ε_{AVG}= 10.204%, is reached for the angle θ equal to $-6°$, whereas in the case of the truss girder, the average error does not exceed 9%, and its maximal value is equal to ε_{AVG} = 17.972% and is obtained for the angle θ equal to 6°. The comparison of the aerodynamic force coefficients from the experiment and numerical simulation is shown in Figures 14 and 15 for the box girder and the truss girder, respectively. It is worth noting the relatively good agreement between the experimental and numerical results. The average value of the average error is satisfactory.

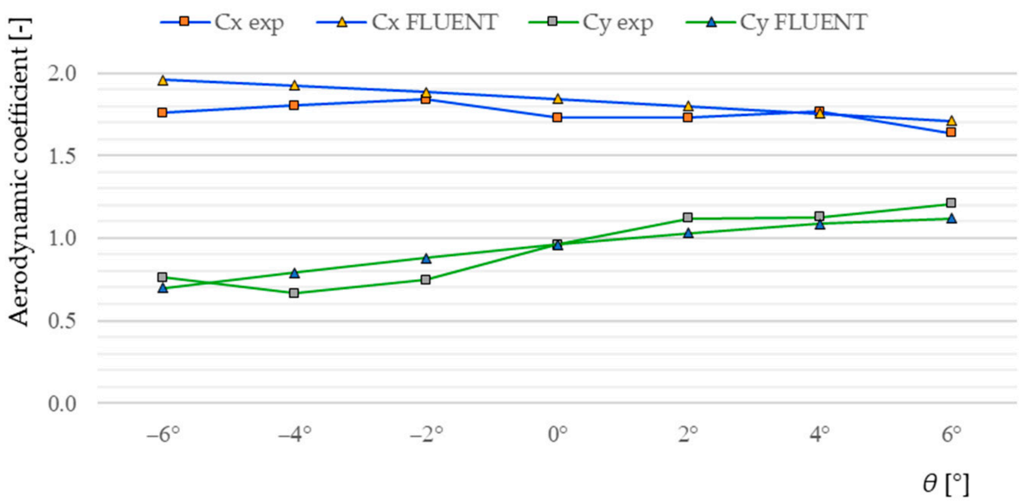

Figure 14. Comparison of C_x and C_y obtained from experiment and CFD for angle θ in the case box girder.

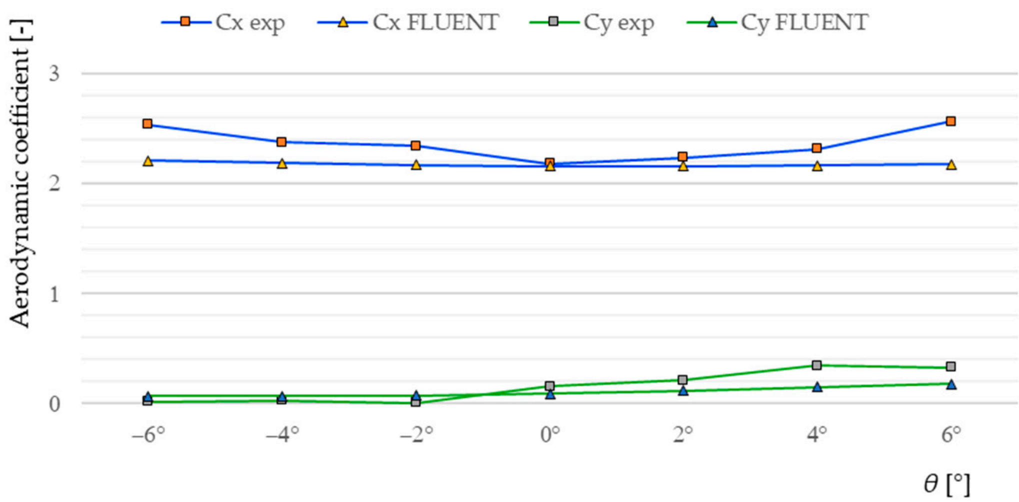

Figure 15. Comparison of C_x and C_y obtained from experiment and CFD for angle θ in the case truss girder.

4. Discussion

4.1. Overturning and Stabilizing Moments Assumed for Gantry Crane According to ISO 4302

Using the resulting coefficients for the box and truss girder model, detailed calculations of the actual ZREMB SB-8 and SBS-4.5 gantry crane stabilities were conducted. The maximum overturning moment M_O and the stabilizing moment M_S were determined concerning the tipping line, which is shown in Figure 16a,b. In the case of a gantry crane, the overturning line is between the supports, i.e., at the circle contact of the crane and rail contact widths. Calculations were conducted for the least favorable wind direction (Figure 16a,b).

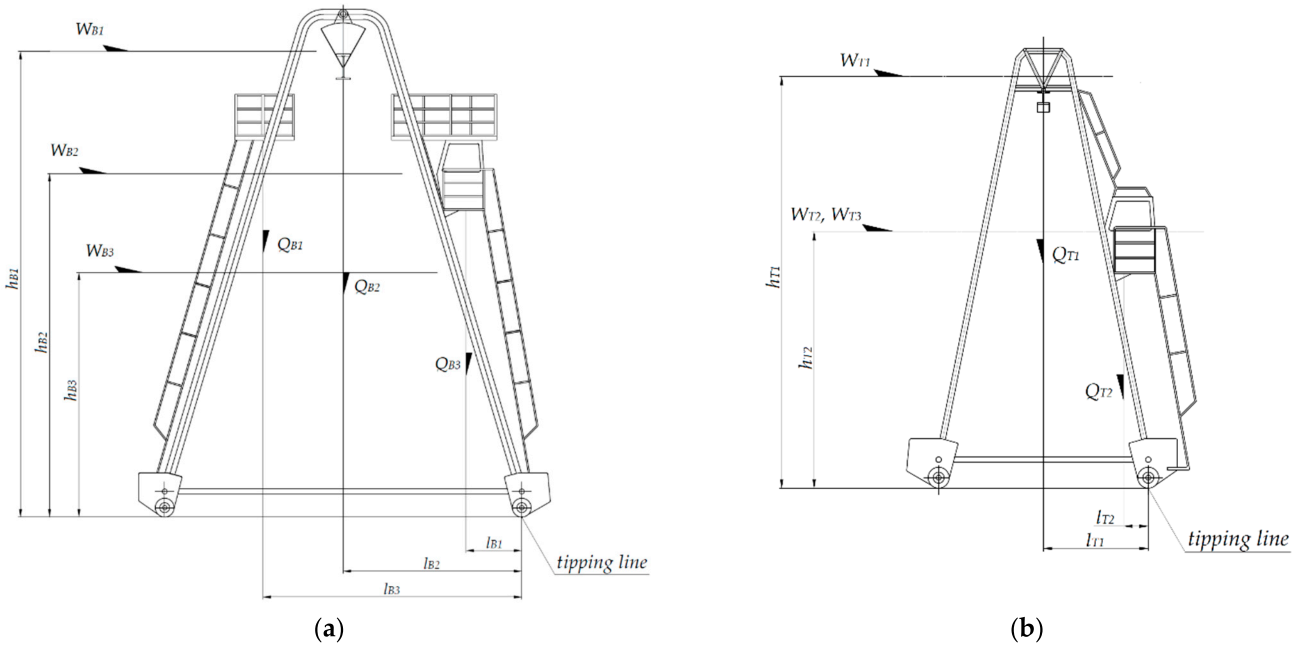

Figure 16. The gantry crane: (**a**) ZREMB SB-8 box girder "B"; (**b**) ZREMB SBS-4.5 truss girder "T".

It was assumed that a crane operating outdoors is affected by a wind pressure of 245 N/m^2, which corresponds to a wind speed of 20 m/s. According to Figure 16a,b, for the stationary gantry crane example with the wheels locked but not coupled to the rail, all loads and forces that can act simultaneously are considered in their most unfavorable combinations. The effective area A_{ref} for the real objects was calculated and yielded the following results for the gantry crane: A_{refB} = A_{refB1} + A_{refB2} + A_{refB3} = 40.24 m^2 for the box girder and A_{refT} = A_{refT1} + A_{refT2} + A_{refT3} = 13.05 m^2 for the truss girder. The effective area was calculated as an area of the perpendicular projection of the structure on the plane, which is perpendicular to the wind direction. The angle attack of the wind was not taken into account.

The self-weight, the components of the effective area, and all the assumed technical parameters of the actual object are presented in Table 5. The masses of the gantry crane elements are assumed as static structural loads Q (stationary), with a factor equal to 1. For dynamic loads, like wind load W, the taken factor is 1.1, according to [48].

Taking the above into account, for the gantry crane to remain stable, the following conditions must be met:

$$M_S > M_O, \tag{5}$$

where M_S is the sum of stabilizing moments; M_O is the sum of overturning moments.

The stabilizing moments for box girder B gantry crane M_{SB} include the following:

$$M_{SB} = M_{SB1} + M_{SB2} + M_{SB3}. \tag{6}$$

M_{SB1} = 625,878.00 Nm, M_{SB2} = 2209.02 Nm, and M_{SB3} = 5687.84 Nm are moments resulting from the product of structural loadings Q_{B1}, Q_{B2}, and Q_{B3}, and distances l_{B1}, l_{B2}, and l_{B3} are those from the tipping line (according to Table 5).

Table 5. Loads and surface areas used for gantry crane stability calculations (B and T girder) for the wind speed of 20 m/s.

	Box Girder			Truss Girder		
	Sign	Value	Description	Sign	Value	Description
Wind load W [N]; horizontal direction	W_{B1}	7897.51	acting on h_{B1} = 10.422 m; girder	W_{T1}	2276.05	acting on h_{T1} = 8.244 m; girder
	W_{B2}	206.49	acting on h_{B2} = 7.69 m; operator's cabin	W_{T2}	206.49	acting on h_{T2} = 5.127 m; operator's cabin
	W_{B3}	1755.98	acting on the arm h_{B3} = 5.477 m; supports and ladders	W_{T3}	714.93	acting on the arm h_{T2} = 5.127 m; supports and ladder
Effective area A_{ref} [m^2]	A_{refB1}	32.23	girder	A_{refT1}	9.29	girder
	A_{refB1}	0.84	operator's cabin	A_{refT2}	0.84	operator's cabin
	A_{refB1}	7.17	supports and ladders	A_{refT3}	2.92	supports and ladder
Structural load Q [kg]; vertical direction	Q_{B1}	15,950	acting on the arm h_{B1} equal to 4.0 m; on girder	Q_{T1}	6875	acting on the arm h_{T1} equal to 2.1 m; girder
	Q_{B2}	180	acting on h_{B2} = 1.251 m; operator's cabin and of the one person	Q_{T2}	180	acting on h_{T2} = 0.492 m; operator's cabin, one person
	Q_{B3}	100	acting on h_{B3} = 5.798 m; supports and ladders	-	-	-

The overturning moments include the following:

$$M_{OB} = M_{OB1} + M_{OB2} + M_{OB3}, \tag{7}$$

M_{OB1} = 90,538.67 Nm, M_{OB2} = 1746.70 Nm, and M_{OB3} = 10,579.27 Nm are moments resulting from the product of wind loadings W_{B1}, W_{B2}, and W_{B3} acting at distances h_{B1}, h_{B2}, and h_{B3}.

Considering the above data, Condition (5) for a box girder B crane for a wind speed of 20 m/s is as follows:

$$M_S = 628,087.02 \text{ Nm} > M_O = 102,864.65 \text{ Nm}, \tag{8}$$

The condition for the stability of the gantry crane is satisfied.

Similarly, the stabilizing moments for the truss girder T gantry crane include the following:

$$M_{ST} = M_{ST1} + M_{ST2}. \tag{9}$$

where $M_{ST1} = Q_{ST1} \cdot l_{T1} = 141,631.88$ Nm; $M_{ST2} = Q_{ST2} \cdot l_{T2} = 141,631.88$ Nm.

The overturning moments include the following:

$$M_{OT} = M_{OT1} + M_{OT2} + M_{OT3}, \tag{10}$$

where $M_{OT1} = W_{T1} \cdot h_{T1} = 20,640.13$ Nm; $M_{OT2} = W_{T2} \cdot h_{T2} = 1164.54$ Nm; $M_{OT3} = W_{T3} \cdot h_{T3} = 4031.98$ Nm.

Condition (5) for a truss crane with a wind speed of 20 m/s is satisfied as follows:

$$M_S = 142,500.65 \text{ Nm} > M_O = 25,836.65 \text{ Nm}. \tag{11}$$

4.2. Influence of the Type of Girder (Its Contour) on the Stability of the Crane Used to Obtain Aerodynamic Coefficients for Three Different Wind Speed

The components of the forces F_x and F_y for the actual object were determined by utilizing the aerodynamic coefficients estimated in the previous study. Considering the components F_x and F_y, the F_X and F_Y forces acting relative to the tipping line of the gantry crane were calculated.

$$F_X = F_x \cos(\beta), \quad F_Y = F_y \sin(\beta), \tag{12}$$

The resultant value of the force F_{rd} and moment M_{Frd} acting relative to the tipping line of the gantry crane was then determined relative to the wind angle θ.

$$F_{rd} = \sqrt{(F_X)^2 + (F_Y)^2}, \quad M_{F_{rd}} = F_{rd} \cdot h_1. \tag{13}$$

The moment M_{Frd} was taken to be a dynamic moment with a factor of 1.1.

The sum of overturning moments from the M_{Oexp} experiment and the $M_{O\,CFD}$ simulation was determined as a function of wind angle θ:

$$M_{Oexp} = M_{Frd\ exp} + M_{O2} + M_{O3}, \qquad M_{O\ CFD} = M_{Frd\ CFD} + M_{O2} + M_{O3}, \tag{14}$$

The calculation results are shown graphically in Figures 17–19 for three example wind speeds V of 20, 30, and 40 m/s. In this case, only the forces from the girder (the girder itself without the cabin, ladders, and housing) were assumed.

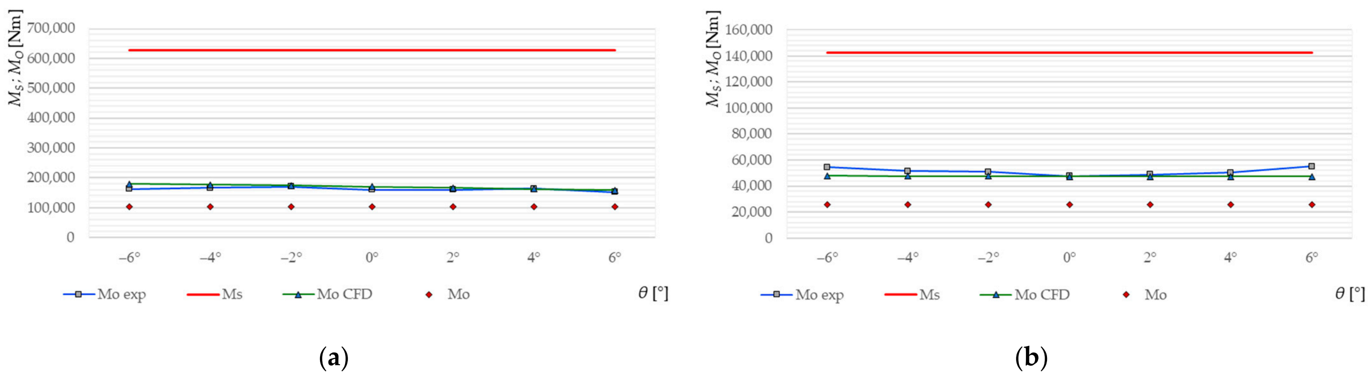

Figure 17. The overturning and stabilizing moments for the wind speed V = 20 m/s: (**a**) the box girder gantry crane; (**b**) the truss girder gantry crane.

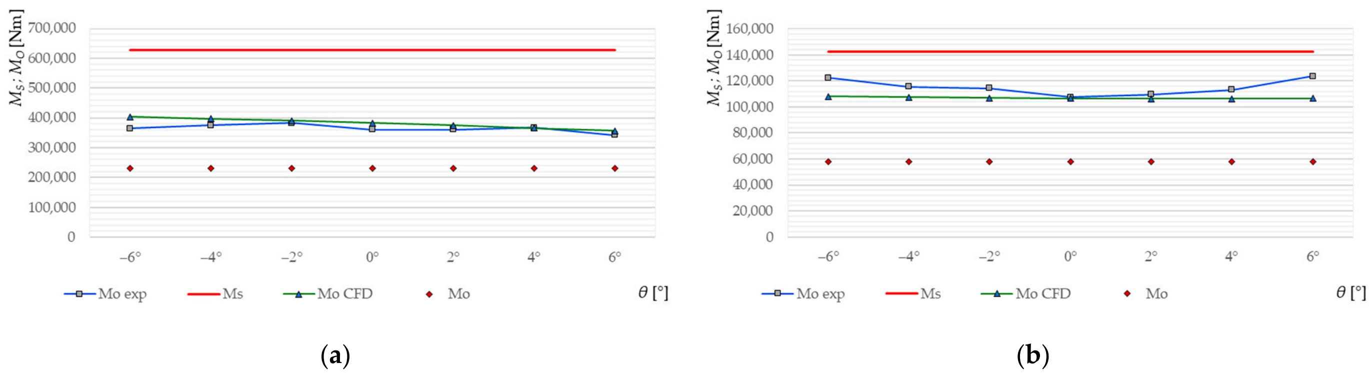

Figure 18. The overturning and stabilizing moments for the wind speed V = 30 m/s: (**a**) the box girder gantry crane; (**b**) the truss girder gantry crane.

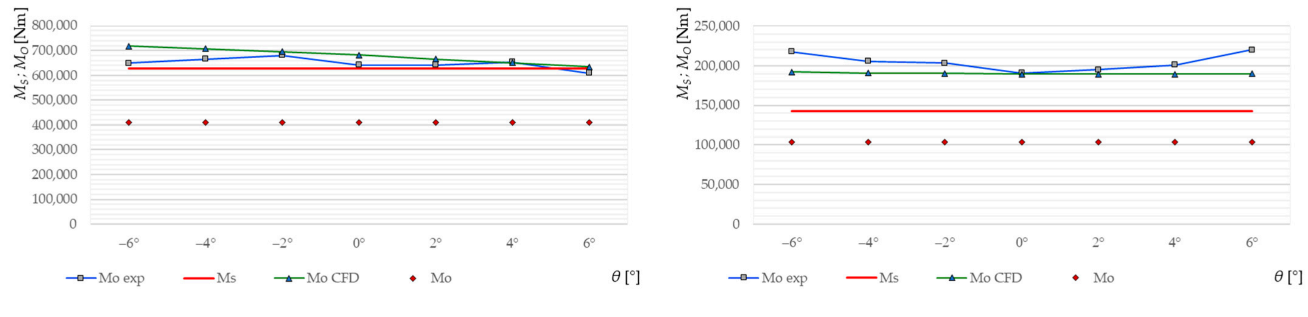

(**a**) (**b**)

Figure 19. The overturning and stabilizing moments for the wind speed V = 40 m/s: (**a**) the box girder gantry crane; (**b**) the truss girder gantry crane.

Considering the above results, it is possible to determine the characteristics of the capsizing moment as a function of wind speed. These graphs are shown in Figure 20. In the case of the box girder, the curves are prepared for the following set of parameters: angle $\theta = -2°$ (experimental), $\theta = -6°$ (CFD simulation). In the case of the truss girder, the curves are prepared for the following set of parameters: θ = 6° (experiment) and θ = −6° (CFD simulation).

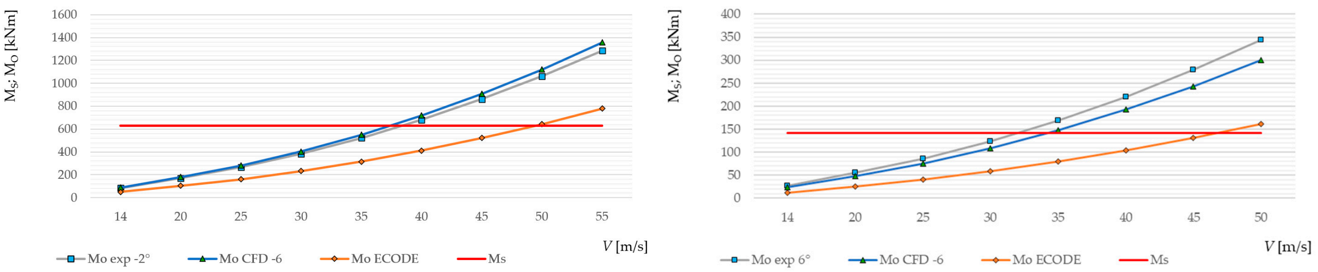

(**a**) (**b**)

Figure 20. Overturning and stabilizing moments for selected wind angles θ compared with the calculations performed according to Eurocode: (**a**) for box girder gantry crane—wind speeds V = 14–55 m/s; (**b**) for truss girder gantry crane—wind speeds V = 14–50 m/s.

According to Figure 20, the gantry crane will be overturned at the approximate wind speed V, as shown in Table 6.

Table 6. The wind speed V for which overturning moments cause loss of stability of the gantry crane (B and T girder).

V	M_O for the Box Girder (Nm)			V	M_O for the Truss Girder (Nm)		
(m/s)	$M_{O\ ECODE}$	$M_{O\ exp}$ −2°	$M_{O\ CFD}$ −6°	(m/s)	$M_{O\ ECODE}$	$M_{O\ exp}$ 6°	$M_{O\ CFD}$ −6°
37.43	-	-	628,117	32.20	-	142,546	-
38.45	-	628,332	-	34.44	-	-	142,583
49.43	628,329	-	-	46.97	142,501	-	-

However, according to the standard [14] and the manufacturer's recommendations, the permissible wind speed for all gantry cranes operating in the open terrain should not exceed 20 m/s (72 km/h).

4.3. Simulation Overturning of the Real-Scale Structure of the Gantry Cranes

Due to the significant difficulty in generating the appropriate FE mesh for the gantry crane with the truss horizontal girder, the computations at real scale were performed only for the gantry crane with the box horizontal girder. The FE model was prepared according to the geometrical dimensions shown in Figure 3a. The simplified model consists of the horizontal girder, left and right support, and the operator's cabin. The gantry crane was placed in a rectangular box filled with air of the following geometrical dimensions: 75 × 105 × 30 m. Like previous studies, the k-ε model was used. The wind speed is assumed to be V = 17.1 m/s, and the turbulent intensity is equal to 12%. The turbulent length scale is assumed to be L_{turb} = 3.5 m. The computations were made for three different Davenport wind profiles, where V_G is a gradient velocity (V_G = 17.1 m/s) measured at z_G height (z_G = 9.89 m). The Davenport wind profile is described with the following formula [14]:

$$V(z) = V_G \left(\frac{Z}{Z_G} \right)^{\alpha}, \tag{15}$$

where the exponent α is equal to 0.4, 0.28, and 0.16 for the urban, village, and open terrain, respectively.

The rest of the parameters are identical to those described above for the sectional model analysis. The assumed minimal element size is equal to 30 mm, and the maximal cell length is approximately equal to 3200 mm. The whole mesh consists of 8,748,698 nodes and 2,135,393 cells. The fragment of the finite cell mesh (faces) created for the box girder is shown in Figure 21, and the whole model (static pressure) is shown in Figure 22.

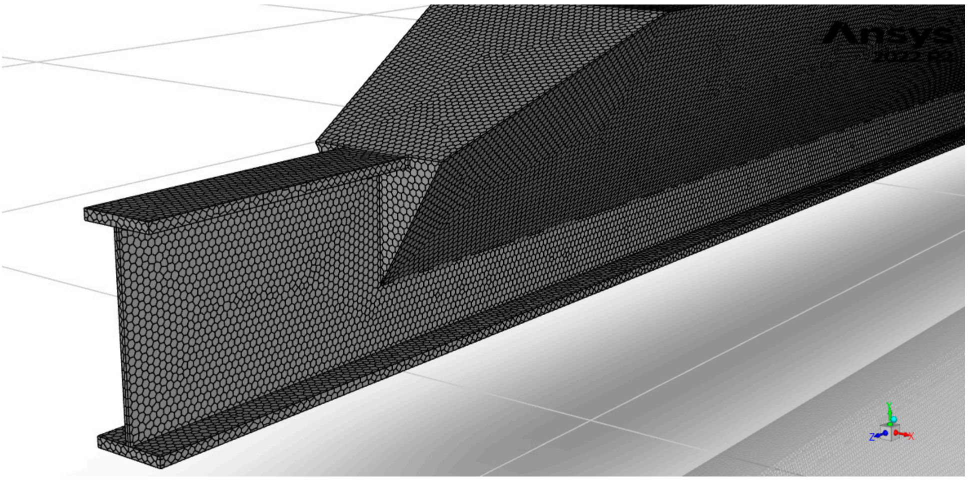

Figure 21. Fragment of the finite cell mesh (faces) created for the box girder.

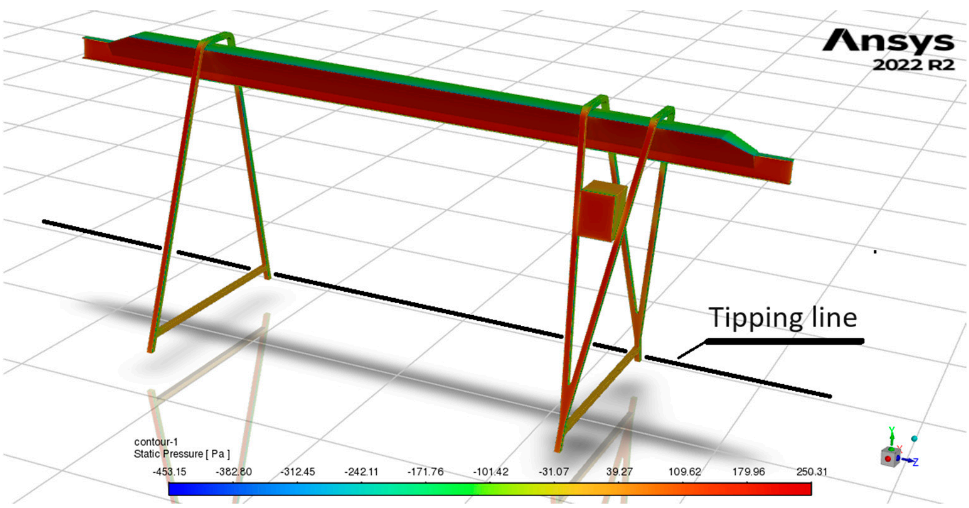

Figure 22. The CFD model of the gantry crane SBS-8 with horizontal box girder. Distribution of static pressure.

In Table 7, the resultant components F_x and F_y of the aerodynamic forces and the overall moment M_z are estimated for the tipping line. The tipping line is shown in Figure 22. As observed, depending on the terrain (in other words, together with the decreasing exponent α in Formula (15)), the values of the F_x force component and the moment M_z slightly increase. Assuming the reference area A_{ref} = 41.106 m² and B_{ref} = 9.89 m, the appropriate moment coefficients can be determined with the following equation:

$$C_M = \frac{M_z}{\frac{1}{2}\rho v^2 A_{ref} B_{ref}}. \tag{16}$$

where exponent α is equal to 0.4, 0.28, and 0.16 for the urban, village, and open terrain, respectively. The appropriate values of coefficient C_M are shown in Table 7.

Table 7. Aerodynamic forces and moments for real-scale structure.

Wind Profile (Terrain)	F_x (N)	F_y (N)	M_z (Nm)	C_M
Urban	11,097.461	4192.185	−121,687.84	1.670
Village	11,353.304	4139.967	−122,673.19	1.683
Open	11,721.647	4080.948	−124,223.43	1.705

The gantry crane would overturn if the moment induced by the wind, computed for the tipping line, were greater than the stabilizing moment, $M_z > M_s$. In the current case, the stabilizing moment is mainly caused by the self-weight of the structure and can be estimated, as shown in Figure 16, as follows:

$$M_s = Q_2 l_{B2} = 714.16 \text{ kNm} \tag{17}$$

Next, the critical wind speed can be computed as follows:

$$V_{cr} = \sqrt{\frac{2M_s}{C_M \rho A_{ref} B_{ref}}} \tag{18}$$

Considering the values of the moment coefficients, as shown in Table 7, the following critical wind speeds, which cause gantry crane overturning, can be obtained: V_1 = 41.445 m/s (149.202 km/h) for urban terrain, V_2 = 41.278 m/s (148.602 km/h) for village terrain, and V_3 = 41.020 m/s (147.672 km/h) for open terrain. The obtained values of the critical wind speed are almost identical, and from a practical point of view, the terrain type has almost no influence on the critical value of the wind speed.

5. Conclusions

This article covers the maximum wind speed at which a gantry crane remains stable. According to the standard [14], the maximum design wind speed V is 20 m/s for all cranes installed in the open. Experimental testing and numerical analysis showed compliance with the standard regarding the stability behavior of this type of structure in open space at an average wind speed of 20 m/s. This study assumed that the gantry crane is stopped but not anchored to the rails on which it moves. For cranes installed in coastal areas, the wind situation is different. The standard states that overhead cranes that must continue to operate in high winds have a maximum design wind speed of 28.5 m/s (102.6 km/h), such as container cranes. In this case, the wind speed for such a facility can range from 20 m/s to 40 m/s (wind speed with gusts of 3 s).

As is reported from the data presented in this paper, the gantry crane with the truss horizontal girder can be overturned at 32.2 m/s (115.92 km/h) of wind speed. On the other hand, the gantry crane with the box girder can be overturned even at 37.45 m/s (134.75) of wind speed. The critical wind speed values obtained from CFD simulations for three different wind profiles and a box girder crane are almost identical and do not depend much on the type of terrain, and the obtained values are V_1 = 41.445 m/s (149.202 km/h) for urban terrain, V_2 = 41.278 m/s (148.602 km/h) for village terrain, and V_3 = 41.020 m/s (147.672 km/h) for the open terrain, which are slightly higher than those determined according to the standards. In other words, estimations based on the standards provide underestimated critical wind speed values; thus, they are safe.

Although the standards provide the magnitudes of the moments regardless of wind direction, the results reported in the current work show significant differences due to the variation in the angle theta. The change in angle theta means that the wind direction is not parallel to the horizontal plane.

Wind strength depends mainly on the geographical location and the degree of wind exposure of the crane, as evidenced by the gantry crane accidents given in the Introduction, among others, including a box crane at the LNG terminal in Swinoujscie [37] (coastal area) and the truss girder crane example described by Frendo [13], where the gantry crane derailed and collapsed after traveling about 60 m in very strong winds of about 30.56 m/s (110 km/h). The given gantry crane disaster examples caused by high winds occurred when the wind speed was comparable to the values reported in this paper.

In this study, the authors wanted to draw attention to the importance of changing wind direction in the vertical plane. Usually, the change in wind direction is considered in the horizontal plane. However, as shown in the results, even a small change in the vertical angle, e.g., only up to 6°, causes significant changes in the value of the overturning moment (for selected angles). Thus, we wanted to show that adopting standard calculations for overhead cranes, which are usually located in urban or non-urban areas but not far from the city, can often lead to accidents, especially when the crane is operated in a coastal (seaside) area.

Author Contributions: Conceptualization, M.A.; methodology, M.A. and M.B.; software, M.B.; validation, M.A. and M.B.; numerical analysis, M.B.; experimental investigation, M.A.; data curation, M.A. and M.B.; writing—original draft preparation, M.A. and M.B; writing—review and editing, M.A. and M.B.; visualization, M.A. and M.B. All authors have read and agreed to the published version of the manuscript.

Funding: This research received no external funding.

Institutional Review Board Statement: Not applicable.

Informed Consent Statement: Not applicable.

Data Availability Statement: Data is contained within the article.

Conflicts of Interest: The authors declare no conflicts of interest.

References

1. Fox Weather. 205-mph Wind Gust from Mexico's Hurricane Otis Ranks as 5th Highest in World. 2023. Available online: http://www.foxweather.com/weather-news/205-mph-wind-gust-hurricane-otis-world-record (accessed on 2 November 2023).
2. Fox Weather. Bomb Cyclone Storm Ciarán Kills 10 as It Slams Europe with Hurricane-Force Winds, Extreme Flooding. 2023. Available online: https://www.foxweather.com/weather-news/bomb-cyclone-storm-ciaran-england-france-hurricane-force-wind (accessed on 2 November 2023).
3. Sports Video Community. Notre Dame's Fatal Scissor Lift Accident Shakes Collegiate. Available online: https://www.athleticbusiness.com/operations/media-technology/article/15142464/notre-dames-fatal-scissor-lift-accident-shakes-collegiate-sports-video-community (accessed on 2 November 2023).
4. Lingard, H.; Cooke, T.; Harley, J.; Pirzadeh, P.; Zelic, G.; Wilczynska, M.; Wakefield, R.; Gharaie, E. *Crane Safety in Construction*; RMIT University, Centre for Work Health and Safety, NSW Department of Customer Service: Melbourne, Australia, 2019.
5. McCarthy, P.; Soderberg, E.; Dix, A. Wind damage to dockside cranes: Recent failures and recommendations. In *Lifeline Earthquake Engineering in a Multihazard Environment. Proceedings of the Technical Council on Lifeline Earthquake Engineering Conference (TCLEE), Oakland, CA, USA, 28 June–1 July 2009*; American Society of Civil Engineers: Reston, VA, USA, 2009.
6. Neitzel, R.L.; Seixas, N.S.; Ren, K.K. A review of crane safety in the construction industry. *Appl. Occup. Environ. Hyg.* **2001**, *16*, 1106–1117. [CrossRef]
7. Zhang, B.; Tong, Y.; Qin, L.; Huang, Z. Research on Wind Disaster Accident of Port Crane. *E3S Web Conf.* **2021**, *257*, 02050. [CrossRef]

8. Weather Build. Rigging for Wind—Common Causes of Tower Crane Accidents. 2019. Available online: http://weatherbuild.co/2019/02/04/rigging-for-wind-common-causes-of-tower-crane-accidents (accessed on 28 March 2023).
9. Express Web Desk. *Watch: Overhead Crane Crashes on Buildings Due to Cyclone Fani*; Express Web Desk: New Delhi, India, 2019; Available online: https://indianexpress.com/article/india/cyclone-fani-overhead-crane-crashes-on-buildings-due-to-severe-storm-5709526/ (accessed on 28 March 2023).
10. Ayub, M.; Lu, A. Investigation of the Failures of Three Hammerhead Cranes on 10 September 2017, in Miami and Fort Lauderdale in the Wake of Hurricane Irma, Office of Engineering Services Directorate of Construction. Youtube. 2018. Available online: https://www.youtube.com/watch?v=LXCj8OmAD4I (accessed on 28 March 2023).
11. Wiosło, M.; Grochot, A. The Gale Overturned a Crane in Krakow. Two People Are Dead, RMF24. 2022. Available online: https://www.rmf24.pl/regiony/krakow/news-wichura-przewrocila-dzwig-w-krakowie-dwie-osoby-nie-zyja-fil,nId,5838306#crp_state=1 (accessed on 28 March 2023). (In Polish)
12. Vertikal.net. Wind Takes Gantry Down. Available online: https://vertikal.net/en/news/story/29691/wind-takes-gantry-down (accessed on 2 November 2023).
13. Frendo, F. Gantry crane derailment and collapse induced by wind load. *Eng. Fail. Anal.* **2016**, *66*, 479–488. [CrossRef]
14. *ISO 4302:2016 EN*; Cranes-Wind Load Assessment. ISO Copyright Office: Geneva, Switzerland, 2016.
15. *BS 2573-1*; British Standard. Rules for the Design of Cranes Part 1: Specifications for Classification, Stress Calculations, and Design Criteria for Structures (4th Revision). BSI: San Jose, CA, USA, 1983.
16. *ASCE SEI 7-22*; Minimum Design Loads and Associated Criteria for Buildings and Other Structures. ASCE: Reston, VA, USA, 2016.
17. *GB/T 3811-2008*; Design Rules for Cranes. General Administration of Quality Supervision, Inspection and Quarantine of the People's Republic of China: Beijing, China, 2008.
18. *JIS B 8830-2001*; Cranes-Wind Assessment. Japanese Industrial Standards Committee: Tokyo, Japan, 2001.
19. *PN-EN 15011+A1:2014-04*; Cranes—Bridge and Gantry Cranes. Polish Committee for Standardization: Warsaw, Poland, 2013.
20. König, G.; Zilch, K.; Lappas, G. Wind loading of shipyard gantry cranes—Full scale measurements. *J. Wind Eng. Ind. Aerodyn.* **1979**, *4*, 429–435. [CrossRef]
21. König, G.; Zilch, K.; Lappas, G. Wind loading of shipyard gantry cranes—A comparison of full-scale measurement, wind tunnel test and gust factor approach, Wind Engineering. In Proceedings of the Fifth International Conference, Fort Collins, CO, USA, 8–13 July 1979; Volume 2, pp. 911–923.
22. Farrugia, R.N.; Sant, T. Modelling wind speeds for cup anemometers mounted on opposite sides of a lattice tower: A case study. *J. Wind Eng. Ind. Aerodyn.* **2013**, *115*, 173–183. [CrossRef]
23. Voisin, D.; Grillaud, G.; Solliec, C.; Beley-Sayettat, A.; Berlaud, J.-L.; Miton, A. Wind tunnel test method to study out-of-service tower crane behavior in storm winds. *J. Wind Eng. Ind. Aerodyn.* **2004**, *92*, 687–697. [CrossRef]
24. Lee, S.J.; Kang, J.H. Wind load on a container crane located in atmospheric boundary layers. *J. Wind Eng. Ind. Aerodyn.* **2008**, *96*, 193–208. [CrossRef]
25. Mara, T.G.; Asce, A.M. Effects of a Construction Tower Crane on the Wind Loading of a High-Rise Building. *J. Struct. Eng.* **2010**, *136*, 1453–1460. [CrossRef]
26. Han, D.S.; Han, G.J. Force Coefficient at Each Support Point of a Container Crane According to the Wind Direction. *Int. J. Precis. Eng. Manuf.* **2011**, *12*, 1059–1064. [CrossRef]
27. Hu, J.B.; Chen, D.; Ding, S.Q.; Qing, G.W. Simulation of the Wind Field of Gantry Cranes Based on FLUENT. *Appl. Mech. Mater.* **2012**, *217–219*, 1530–1534. [CrossRef]
28. Wang, Y.P.; Cheng, W.M.; Du, R.; Wang, S.B.; Yang, X.Z.; Zhai, S.C. Simulation analysis of wind load response for large gantry crane. *Chin. J. Eng. Des.* **2020**, *27*, 239–246.
29. Zan, Y.F.; Guo, R.N.; Bai, X.; Ma, Y.; Yuan, L.H.; Huasng, F.X. Wind and current loads on a pipelaying crane vessel. *IOP Conf. Ser. Earth Environ. Sci.* **2020**, *612*, 012059. [CrossRef]
30. ANSYS, Inc. Fluent (Version R22), Canonsburg, PA, USA. Available online: https://www.ansys.com/products (accessed on 17 January 2023).
31. Romanello, G. Stability analysis of mobile cranes and determination of outriggers loading. *J. Eng. Des. Technol.* **2018**, *16*, 938–958. [CrossRef]
32. El Ouni, M.H.; Ben Kahla, N.; Islam, S.; Jameel, M. A Smart Tower Crane to Mitigate Turbulent Wind Loads. *Struct. Eng. Int.* **2019**, *31*, 18–29. [CrossRef]
33. Chen, W.; Qin, X.; Yang, Z. A mathematical model for the along-wind coefficient of tower crane based on the member load. *Wind Struct.* **2023**, *37*, 347–359.
34. Skelton, I.; Demian, P.; Glass, J.; Bouchlaghem, D.; Anumba, C. Lifting Wing in Constructing Tall Buildings—Aerodynamic Testing. *Buildings* **2014**, *4*, 245–265. [CrossRef]
35. Cekus, D.; Gnatowska, R.; Kwiatoń, P. Impact of Wind on the Movement of the Load Carried by Rotary Crane. *Appl. Sci.* **2019**, *9*, 3842. [CrossRef]
36. Cekus, D.; Kwiatoń, P.; Geisler, T. The dynamic analysis of load motion during the interaction of wind pressure. *Meccanica* **2021**, *56*, 785–796. [CrossRef]
37. Siwek, D. The Wind Damaged the LNG Terminal in Świnoujście. Available online: https://radioszczecin.pl/1,361858,wiatr-uszkodzil-terminal-lng-w-swinoujsciu (accessed on 29 October 2017). (In Polish)

38. Augustyn, M.; Barski, M.; Chwał, M.; Stawiarski, A. Numerical and Experimental Determination of the Wind Speed Value Causing Catastrophe of the Scissor Lift. *Appl. Sci.* **2023**, *13*, 3528. [CrossRef]
39. Augustyn, M.; Barski, M.; Chwał, M.; Stawiarski, A. Experimental and Numerical Estimation of the Aerodynamic Forces Induced by the Wind Acting on a Fast-Erecting Crane. *Appl. Sci.* **2023**, *13*, 10826. [CrossRef]
40. Wind Engineering Laboratory. Available online: http://www.windlab.pl/en/ (accessed on 20 February 2023).
41. *EN 1991-1-4*; Eurocode 1: Actions on Structures—Part 1–4: General Actions—Wind Actions. [Authority: The European Union Per Regulation 305/2011, Directive 98/34/EC, Directive 2004/18/EC]. CEN: Brussels, Belgium, 2005. (In English)
42. Chen, W.; Qin, X.; Yang, Z.; Zhan, P. Wind-induced tower crane vibration and safety evaluation. *J. Low Freq. Noise Vib. Act. Control* **2020**, *39*, 297–312. [CrossRef]
43. Lu, Y.; Gao, M.; Liang, T.; He, Z.; Feng, F.; Pan, F. Wind-induced vibration assessment of tower cranes attached to high-rise buildings under construction. *Automat. Constr.* **2022**, *135*, 104132. [CrossRef]
44. Wu, X.; Sun, Y.; Wu, Y.; Su, N.; Peng, S. The Interference Effects of Wind Load and Wind-Induced Dynamic Response of Quayside Container Cranes. *Appl. Sci.* **2022**, *12*, 10969. [CrossRef]
45. Monteiro, F.A.; Moreira, R.M. A CFD Analysis of Wind Effects on Lifted Loads. *Int. J. Adv. Eng. Res. Sci.* **2019**, *6*, 365–371. [CrossRef]
46. He, Z.; Gao, M.; Liang, T.; Lu, Y.; Lai, X.; Pan, F. Tornado-affected safety assessment of tower cranes outer-attached to super high-rise buildings in construction. *J. Build. Eng.* **2022**, *51*, 104320. [CrossRef]
47. Yeon, S.M.; Kwon, C.S.; Kim, Y.C.; Kim, K.S. Study of the lift effect on wind load estimation for a semi-submersible rig using the maritime atmospheric boundary layer model. *Int. J. Nav. Archit. Ocean Eng.* **2022**, *14*, 100419. [CrossRef]
48. *ISO 8686-5:1992*; Cranes. Design Principles for Loads and Load Combinations. Part 5: Overhead Travelling and Portal Bridge Cranes. ISO Copyright Office: Geneva, Switzerland, 1992.